Synthesis and characterization of fluoride-incorporated polyoxovanadates

Synthesis and characterization of fluoride-incorporated polyoxovanadates

Yuji Kikukawa, Taiga Yokoyama, Sanae Kashio, Yoshihito Hayashi*

Department of Chemistry, Graduate School of Natural Science and Technology, Kanazawa University,

Kakuma, Kanazawa 920-1192, Japan

* Corresponding author. Fax: +81-76-264-5742

E-mail addresses: hayashi@se.kanazawa-u.ac.jp

ABSTRACT

The speciation studies of oxovanadates are essential to clarify their biological activities. We surveyed the distribution of oxovanadate species in the presence of halide anions with various acid concentrations in an aqueous mixed-solvent system. The presence of chloride, bromide, and iodide anions has no effects on the appearance of polyoxovanadate species observed in ^{51}V NMR. Those are precedented formation of metavanadate species and decavanadates. The presence of fluoride anion during the addition of acids exhibits the strong intervention in the polyoxovanadate equilibria and we found the subsequent formation of two polyoxovanadate species by ^{51}V NMR observation. From the estimated experimental condition, we isolated fluoride-incorporated polyoxovanadates $\{Et_4N\}_4[V_7O_{19}F]$ and $\{Et_4N\}_4[HV_{11}O_{29}F_2]$, successfully. Polyanion $[V_7O_{19}F]^{4-}$ is the fluoride-incorporated all V(V) state polyoxovanadate which has two different coordination environments of tetrahedral and square pyramidal vanadium units within the one anionic structural integrity. The structural gap between tetrahedral-unit-based metavanadate and octahedral-unit based decavanadate structure may be linked by this hybrid complex.

Keywords: Polyoxovanadate, Vanadium, Fluoride, Anion capture, Structure transformation

1. Introduction

Oxovanadates, VO_4^{3-}, in oxidation state (V) have long been recognized as an analogue of phosphate, PO_4^{3-} [1]. These oxo-anions show similar stepwise protonation and subsequent oligomerization. The structural similarity allows oxovanadates to interact with a biological system through phosphate-dependent metabolic processes [2-4]. Pharmacological properties of oxovanadates such as enzyme inhibitors and insulin-enhancing agents have been investigated [2-4]. An important difference between oxovanadates and phosphates is the preference of the coordination spheres. Oxovanadates readily form decavanadates, $[V_{10}O_{28}]^{6-}$, that is composed of VO_6 octahedral coordination spheres, while phosphates prefer tetrahedral PO_4 coordination sphere, exclusively. For oxovanadates, the solution system involves equilibria with mono-, di-, tri-, tetra-, penta-, and decavanadates [5]. One of the interesting utilization of oxovanadates is developed by Crans's group. Once decavanadates are placed in micelles, it may interact with hydrophobic or hydrophilic sites, under the condition with a limited amount of water [6-9]. In such a confined-space, the chemical equilibrium may lead to a different distribution with a new species in-between metavanadates and decavanadates.

Oxovanadates can interact with some biological tissue and have the potential to play a role in the treatment of e.g. ulcers, cancer, and ischemic heart disease [10-14]. The biological reactivity of oxovanadates depends on which species is present in the solution [15]. Therefore, the speciation studies of oxovanadates are essential to clarify their biological activities. Up to now, some reports on the speciation of oxovanadates under the biomimetic conditions, e.g. in the presence of chloride and phosphate anions, have been reported suggesting that the effects of simple anions are significant [16-18]. Although fluoride anions can be assimilated into the body through some kinds of tea, water, and tooth paste, the distribution of oxovanadates in the presence of fluoride anions remains largely unexplored.

We have studied the effects of halide anions for the polyoxovanadate syntheses in acetonitrile

solution and found a few polyoxovanadate species such as $[HV_{11}O_{29}F_2]^{4-}$ and $[HV_{12}O_{32}(Cl)]^{4-}$ [19]. In this study, we investigated acidification of metavanadates in the presence of fluoride anions in a mixed solvent of acetonitrile and water, which simulate the reaction in a limited amount of water with controlled proton concentration. This study leads to a discovery of rational syntheses of $[V_7O_{19}F]^{4-}$and $[HV_{11}O_{29}F_2]^{4-}$. The successful isolation of the products allows the full characterization by X-ray crystallography, IR, ^{51}V and ^{19}F NMR, UV/visible (UV/Vis), and cyclic voltammetry.

2. Experimental section

2.1. Physical measurements

IR spectra were measured on Jasco FT/IR-4100 using KBr disks. NMR spectra were recorded with JEOL JNM-LA400. ^{51}V and ^{19}F NMR spectra were measured at 105.15 and 376.17 MHz, respectively. All spectra were obtained in the solvent indicated, at 25ºC unless otherwise noted. ^{19}F NMR spectra were referenced to neat CF_3COOH (δ = 0.00). ^{51}V NMR spectra were referenced using a sample of 10 mM $NaVO_3$ in 2.0 M NaOH (−541.2 ppm). UV/Vis spectra were recorded using a Hitachi U-3500 spectrophotometer. An ALS/CH Instruments electrochemical analyzer (Model 600A) was used for voltammetric experiments. The working electrode was glassy carbon, the counter electrode was Pt wire, and the reference electrode was Ag/Ag^+. The voltage scan rate was set at 100 mV s^{-1}. The potentials in all voltammetric experiments were converted using data derived from the oxidation of Fc (Fc/Fc^+, Fc = ferrocene) as an external reference. Elemental analyses of C, H, and N were performed by the Research Institute for Instrumental Analysis at Kanazawa University. Elemental analysis of F were performed by the Center for Organic Elemental Microanalysis Laboratory at Kyoto University.

2.2. NMR studies for the effect of the presence of halide anions on the distribution of oxovanadate species

$\{Et_4N\}_4[V_4O_{12}]\cdot 2H_2O$ (238 mg, 0.25 mmol) and $\{n\text{-}Bu_4N\}X$ (0.20 mmol, X = F^-, Cl^-, Br^-, or I^-) was dissolved in a mixed solvent of acetonitrile and water (3:1, v/v). Then, the required amounts of 2.0 M *p*-toluenesulfonic acid (TsOH) acetonitrile/water solution (3:1, v/v) were added. The dissolved species was monitored by ^{51}V NMR.

2.3. Synthesis

2.3.1. Materials

The chemicals and reagents were purchased from various commercial sources and were used without further purification unless otherwise stated. $\{Et_4N\}_4[V_4O_{12}]\cdot 2H_2O$ was synthesized according to the reported procedure [20].

2.3.2. Synthesis of $\{Et_4N\}_4[V_7O_{19}F]$

To an acetonitrile solution of $\{Et_4N\}_4[V_4O_{12}]$ (0.25 mmol, 2 mL), $\{n\text{-}Bu_4N\}F\cdot 3H_2O$ (45 mg, 0.14 mmol) and $TsOH\cdot H_2O$ (108 mg, 0.57 mmol) were added. The solution was filtered and the filtrate was kept for several hours at 5ºC, giving orange crystals suitable for X-ray crystallographic analysis (91 mg, 53% yield based on V). Anal. Calcd. for $\{Et_4N\}_4[V_7O_{19}F]$: C, 32.01; H, 6.72; N, 4.67; F, 1.58; found: C, 31.93; H, 6.84; N, 4.55; F, 1.62. IR (KBr pellet; 4000−400 cm^{-1}): 3419, 2984, 2950, 1636, 1486, 1456, 1441, 1394, 1369, 1305, 1174, 1122, 1069, 1057, 1005, 955, 930, 931, 788, 622, 562, and 448 cm^{-1}. ^{51}V NMR (105.15 MHz, propylene carbonate/dichloromethane-d_2, 1:1, v/v, 25°C): δ −453, −541, and −605 ppm. ^{19}F NMR (376.17 MHz, propylene carbonate/ dichloromethane-d_2, 1:1, v/v, 25°C): δ −71 ppm.

2.3.3 Synthesis of {Et$_4$N}$_4$[HV$_{11}$O$_{29}$F$_2$]

To an acetonitrile solution of {Et$_4$N}$_4$[V$_4$O$_{12}$] (0.25 mmol, 2 mL), {*n*-Bu$_4$N}F·3H$_2$O (57 mg, 0.18 mmol) and TsOH·H$_2$O (156 mg, 0.82 mmol) were added. The solution was filtered and the filtrate was kept for several hours, giving red crystals (91 mg, 63% yield based on V). Anal. Calcd. for {Et$_4$N}$_4$[HV$_{11}$O$_{29}$F$_2$]: C, 24.26; H, 5.15; N, 3.54; found: C, 24.76; H, 5.33; N, 3.59. IR (KBr pellet; 4000−400 cm^{-1}): 3446, 2981, 2951, 1635, 1484, 1458, 1391, 1374, 1308, 1184, 1118, 1080, 1056, 1010, 987, 965, 853, 792, 732, 651, and 486 cm^{-1}. ^{51}V NMR (105.15 MHz, propylene carbonate/CD_2Cl_2, 1:1, v/v, 25°C): δ −466, −470, −488, −502, −527, and −536 ppm. ^{19}F NMR (376.17 MHz, propylene carbonate/CD_2Cl_2, 1:1, v/v, 25°C): δ −67 ppm (d, $J_{F,F}$ = 50 ± 20 Hz) and −72 ppm (d, $J_{F,F}$ = 50 ± 20 Hz).

2.4. X-ray Crystallographic analysis

Single crystal structure analysis was performed at −150ºC by using a Rigaku/MSC Mercury diffractometer with graphite monochromated Mo Kα radiation (λ = 0.71069 Å) and with 0.5º ω-scans at 0º and 90º in φ. The crystal data is summarized in Table 1. Data were collected and processed by using the CrystalClear program [21]. Numerical absorption corrections were applied by using CrystalClear and corrections for Lorenz and polarization effects were performed. The structure analysis was performed using CrystalStructure [22]. All structures were solved by SHELXS-97 (direct methods) and refined by SHELXL-2013 [23,24]. Non-hydrogen atoms were refined anisotropically. Hydrogen atoms are positioned geometrically and refined using a riding model.

3. Results and discussion

3.1. Distribution studies in the presence of halide anions

The vanadium speciation in aqueous solution have been well established. In the neutral pH, mono-, di- tetra- and pentavanadate species are distributed in equilibrium, and in acidic condition, decavanadates are preferably formed [16-18,25]. The vanadium chemistry in an organic solution is quite different from that in an aqueous solution. In an organic solution, various polyoxovanadate species such as $[V_5O_{14}]^{3-}$, $[PdV_6O_{18}]^{4-}$, $[Cu_2V_8O_{24}]^{4-}$, $[Mn_2(V_5O_{15})_2]^{6-}$, $[Co_2(OH_2)_2V_{10}O_{30}]^{6-}$, $[HTeV_9O_{28}]^{4-}$, and $[V_{12}O_{32}Cl]^{5-}$, which could not be obtained in an aqueous solution, have been synthesized by using $[V_4O_{12}]^{4-}$ as a precursor [26-29]. Recent studies in our laboratory have focused on the exploration of a mixed solvent system with water, which mimic the confinement environment surrounded by organic compounds and water at the same space in a biological system.

To survey the effect of halide anions on the distribution of oxovanadate species, proton concentration was varied by the addition of 0 to 3.4 equivalents of *p*-toluenesulfonic acid (TsOH) with fluoride, chloride, bromide, or iodide anions. As a control experiment, the same experiment without halide anions was carried out. $\{Et_4N\}_4[V_4O_{12}]$ was dissolved in a mixed solvent of acetonitrile and water (3:1, v/v). ^{51}V NMR spectrum showed two signals at −585 and −596 ppm due to $[V_4O_{12}]^{4-}$ and $[V_5O_{15}]^{5-}$, respectively (Fig. 1). By the addition of 1.1 equivalents of TsOH, signals at −423 , −500, and −519 ppm due to a decavanadate were observed. By the addition of 1.7 equivalents of TsOH, intensity ratio of the signals due to a decavanadate increased. Signals at −601 and −608 ppm were assigned as the signals from $[V_{12}O_{32}(CH_3CN)]^{4-}$ [30]. Further addition of TsOH (2.4 equivalents) yielded the yellow precipitate of $\{Et_4N\}_3[H_3V_{10}O_{28}]$, which was estimated by IR spectrum (Fig. S1). These distribution of vanadium species depending on the acid concentration closely resembled the distribution in water, without the formation of dodecavanadate [25].

To the $\{Et_4N\}_4[V_4O_{12}]$ solution in the presence of 0.8 equivalents of $\{n\text{-}Bu_4N\}Cl$, $\{n\text{-}Bu_4N\}Br$, or $\{n\text{-}Bu_4N\}I$, the addition of 1.7 equivalents of TsOH gave almost the same spectra

as that of the control experiment, showing that Cl^-, Br^-, and I^- have no effect on the vanadium speciation (Fig. S2). On the other hand, in the presence of 0.8 equivalents of {*n*-Bu_4N}F, the acidified solution gave novel three signals at −460, −547, and −611 ppm without those due to decavanadates (Fig. 2). By the addition of 1.7 equivalents of TsOH with respect to $[V_4O_{12}]^{4-}$, ^{51}V NMR spectrum showed clearly three signals with intensity ratio of 3:3:1 and ^{19}F NMR spectrum showed the main signal at −74 ppm (Fig. S3), indicating the emergence of a fluoride-incorporated polyoxovanadate. Successive addition of acids gave six signals at −471, −474, −492, −505, −530, and −540 ppm in ^{51}V NMR and two signals at −68 and −73 ppm in ^{19}F NMR, suggesting the consecutive formation of $[HV_{11}O_{29}F_2]^{4-}$ (Fig. 2 and S2) [19]. Thus, fluoride anions had the significant effect on the vanadium speciation in an aqueous mixed solvent.

3.2. Synthesis and X-ray structure of {Et_4N}$_4$[$V_7O_{19}F$]

From the above results, we estimated the best experimental condition for the synthesis of $[V_7O_{19}F]^{4-}$. Addition of 0.57 equivalents of {*n*-Bu_4N}F and 2.3 equivalents of TsOH into the acetonitrile solution of {Et_4N}$_4$[V_4O_{12}] gave orange crystals of {Et_4N}$_4$[$V_7O_{19}F$] (53% yield based on V). The molecular structure was determined by X-ray crystallographic analysis (Fig. 3). The selected bond lengths and the crystallographic data were summarized in Table 1 and S1, respectively. Four tetraethylammonium cations per one anion were crystallographically assigned in accord with the result of the elemental analysis. The bond valence sum values of vanadium atoms (4.95−5.03) indicates that the valences of these atoms are fully oxidized V(V) state [31]. Polyanion $[V_7O_{19}F]^{4-}$ possessed one fluoride anion at the center position surrounded by seven vanadium atoms. The shortest V···F distance of $[V_7O_{19}F]^{4-}$ (2.31 Å) is longer than that of the usual V−F bonds (ca. 1.8Å), suggesting that vanadium atoms and a fluoride anion are not directly bonded (Table 1). Very recently, Omri and co-workers reported {Et_2H_2N}$_4$[$V_7O_{19}F$], which possessed the same anion structure as that of {Et_4N}$_4$[$V_7O_{19}F$]. It was obtained from the mixture of vanadium

oxide with hydrofluoric acid and diethylamine in the presence of fumaric acid in water after four months of slow evaporation [32]. Our investigation in pure water revealed that the addition of 1.1 equivalents of TsOH with respect to $\{Et_4N\}_4[V_4O_{12}]$ in the presence of $\{n\text{-}Bu_4N\}F$ gave the mixture of metavanadate, decavanadate, and $\{Et_4N\}_4[V_7O_{19}F]$ (Fig. S4). In our synthetic method, which utilizes the condition of the organic solvent with a limited amount of water, dissolved species can be controlled exclusively as a single species and the desired product can be obtained in a few hours with high yield. Although some fluoride-incorporated polyoxovanadates, such as $[V_7O_{18}F(CH_2)_3CCH_2OH]^{4-}$, $[V_{14}O_{36}F_4]^{8-}$, $[V_{12}O_{30}F_2\{(CH_2)_3CCH_2OH\}_2]^{6-}$, $[V_{10}O_{28}F_2\{(CH_2)_3CCH_2OH\}_2]^{4-}$, $[V_6O_6F(OH)_3\{(OCH_2)_3CCH_3\}_3]^{-}$ $[V_8O_8(OCH_3)_{16}(VOF_4)]^{2-}$, $[V_4(HPO_4)(PO_4)_3O_6F]^{4-}$, $[H_6V_{12}O_{30}F_2]^{6-}$, and $[V_{16}O_{38}F]^{4-}$ were reported until now [33-39], only $[V_7O_{19}F]^{4-}$ and $[HV_{11}O_{29}F_2]^{4-}$ were composed of fully oxidized vanadium atoms without any reduced vanadium atoms. X-ray crystallographic and elemental analyses show that the formula is $\{Et_4N\}_4[V_7O_{19}F]$. The formation of $[V_7O_{19}F]^{4-}$ can be expressed by the following reaction (1).

$$7[V_4O_{12}]^{4-} + 4F^- + 16H^+ \rightarrow 4[V_7O_{19}F]^{4-} + 8H_2O \qquad (1)$$

The vanadium atoms in $[V_7O_{19}F]^{4-}$ can be classified into three types (V_{bottom}, V_{middle}, and V_{top}). The V_{bottom} atoms (V1, V2, and V3) represent the square pyramidal geometry. The V_{middle} (V4, V5, and V6) and V_{top} (V7) atoms show tetrahedral geometry. The V_{middle} atoms are sandwiched by V_{bottom} and V_{top} atoms. In general, fully oxidized polyoxovanadates adopt only one kind of vanadium coordination geometry within the one anionic structural integrity [20,29,30,40-57]. For example, all vanadium atoms in circular polyoxovanadates adopt tetrahedral geometry [20,40-50]. Spherical vanadates and decavanadates adopt square pyramidal and octahedral geometries, respectively [29,30,51-55].

The three VO_5 and four VO_4 units are joined at vertexes to form the cage structure in such a way that the entire anion adopts approximately C_{3v} symmetry. The average bond length of the

bridging oxygen atoms interlinking V_{bottom} atoms is 1.83 Å with the small deviation (±0.01 Å). On the other hand, the oxygen atoms interlink V_{bottom} and V_{middle} atoms, and V_{middle} and V_{top} atoms asymmetrically. The V_{bottom}–O–V_{middle} sites show the longer average V_{bottom}–O bond length (1.97 Å) than that of V_{middle}–O (1.72 Å). As for V_{middle}–O–V_{top}, the average V_{middle}–O bond length (1.84 Å) is longer than that of V_{top}–O (1.76 Å). These values were almost the same as the reported heptavanadate [32]. The average $V_{bottom}\cdots V_{bottom}$, separation of $[V_7O_{19}F]^{4-}$ (3.14 Å) is shorter than that of $[V_7O_{18}F(CH_2)_3CCH_2OH]^{4-}$ (3.37 Å) due to the valence and the absence of the alkoxide ligands. The position of a fluoride anion of $[V_7O_{19}F]^{4-}$ is slightly different from that of $[V_7O_{18}F(CH_2)_3CCH_2OH]^{4-}$. A fluoride anion of $[V_7O_{19}F]^{4-}$ is located in the same plane defined by six oxygen atoms bridging V_{bottom} and V_{middle} atoms, while that of $[V_7O_{18}F(CH_2)_3CCH_2OH]^{4-}$ is slightly under the plane (0.25 Å). As a result, the average $V_{bottom}\cdots F$ separation of $[V_7O_{19}F]^{4-}$ (2.31 Å) are slightly longer than that of $[V_7O_{18}F(CH_2)_3CCH_2OH]^{4-}$ (2.20 Å), and the $V_{middle}\cdots F$ and $V_{top}\cdots F$ separations of $[V_7O_{19}F]^{4-}$ (2.76 Å and 2.97 Å) are shorter than those of $[V_7O_{18}F(CH_2)_3CCH_2OH]^{4-}$ (2.94 Å and 3.24 Å), respectively (Table 2). These geometrical comparisons show the cage size of $[V_7O_{19}F]^{4-}$ is smaller than that of the $[V_7O_{18}F(CH_2)_3CCH_2OH]^{4-}$, which possess the reduced vanadium atoms.

3.3. Synthesis of $\{Et_4N\}_4[HV_{11}O_{29}F_2]$

We have reported the synthesis and X-ray crystallographic analysis of $\{n\text{-}Bu_4N\}_4[HV_{11}O_{29}F_2]$. In the reported procedure, oxidation step was necessary [19]. The preliminary distribution experiment by ^{51}V NMR revealed that $[HV_{11}O_{29}F_2]^{4-}$ is produced directly from $[V_4O_{12}]^{4-}$ via reaction (2) without reduction and oxidation process.

$$11[V_4O_{12}]^{4-} + 8F^- + 36H^+ \rightarrow 4[HV_{11}O_{29}F_2]^{4-} + 16H_2O \qquad (2)$$

Addition of 7.3 equivalents of {*n*-Bu_4N}F and 3.3 equivalents of TsOH with respect to $[V_4O_{12}]^{4-}$ into the acetonitrile solution of $\{Et_4N\}_4[V_4O_{12}]$ gave $\{Et_4N\}_4[HV_{11}O_{29}F_2]$ (63% yield based on V). The formation of $[HV_{11}O_{29}F_2]^{4-}$ was confirmed by ^{51}V and ^{19}F NMR spectra. The elemental analysis show that the formula is $\{Et_4N\}_4[HV_{11}O_{29}F_2]$.

Resemblance between $[V_7O_{19}F]^{4-}$ and $[HV_{11}O_{29}F_2]^{4-}$ is shown in Fig. 4. The structural half of $[HV_{11}O_{29}F_2]^{4-}$, composed of one cap layer and three vanadium atoms in the belt layer, is similar to the structure of $[V_7O_{19}F]^{4-}$ without VO_4 unit on the top of $[V_7O_{19}F]^{4-}$. The removal of one VO_4 unit from the top of $[V_7O_{19}F]^{4-}$ gives a $[V_6O_{15}F]^{-}$ unit and the dimerization followed by the removal of VO unit gives $[HV_{11}O_{29}F_2]^{4-}$ (Fig. 4).

3.4. Spectroscopic and electrochemical analyses

IR spectrum of $[V_7O_{19}F]^{4-}$ shows several bands in the range of 920-960 cm^{-1} due to terminal V−O stretching frequencies and very strong bands around 830 cm^{-1} due to V−μ-O stretching frequencies. These band intensities and positions are similar to those of$[V_7O_{18}F(CH_2)_3CCH_2OH]^{4-}$ (Fig. S5) [33]. The band positions assigned to the terminal V−O stretching frequencies of $[HV_{11}O_{29}F_2]^{4-}$ (987 and 964 cm^{-1}) are different from those of $[V_7O_{19}F]^{4-}$. The spectrum shape of $[HV_{11}O_{29}F_2]^{4-}$ resembles that of $[V_{14}O_{36}F_4]^{8-}$ which possess the similar anion structure (Fig. S5) [34]. The higher wavenumber shift of V−μ-O stretching frequencies in $[HV_{11}O_{29}F_2]^{4-}$ is observed due to the absence of reduced vanadium units.

NMR spectroscopic analyses of isolated $\{Et_4N\}_4[V_7O_{19}F]$ and $\{Et_4N\}_4[HV_{11}O_{29}F_2]$ were investigated. In a mixed solvent of acetonitrile and water used in the distribution study, $\{Et_4N\}_4[HV_{11}O_{29}F_2]$ was not stable while $\{Et_4N\}_4[V_7O_{19}F]$ was stable. To prevent the decomposition of both $\{Et_4N\}_4[V_7O_{19}F]$ and $\{Et_4N\}_4[HV_{11}O_{29}F_2]$, a mixed solvent of propylene carbonate and dichloromethane was used. ^{51}V NMR spectrum of $\{Et_4N\}_4[V_7O_{19}F]$ showed three signals at –453, –541, and −605 ppm with the respective intensity ratio of 3:3:1 as shown in Fig.

4. ^{19}F NMR spectrum of $\{Et_4N\}_4[V_7O_{19}F]$ showed single signals at –71 ppm. These results suggested that the solid state structure of $[V_7O_{19}F]^{4-}$ preserves in the solution state. ^{51}V NMR spectrum of $\{Et_4N\}_4[HV_{11}O_{29}F_2]$ showed six signals at –462, –467, –485, –499, –525, and –533 ppm with an intensity ratio of 1:2:3:1:2:2 without any signals due to decomposition products. ^{19}F NMR spectrum of $\{Et_4N\}_4[HV_{11}O_{29}F_2]$ showed two doublet peaks at −67 and−72 ppm, respectively with $J = 50 \pm 20$ Hz, which was attributed to F−F coupling in the encapsulated fluoride anions (Fig. 4).

UV/Vis spectrum of $\{Et_4N\}_4[V_7O_{19}F]$ in a mixed solvent of propylene carbonate and dichloromethane (1:1, v/v) showed a shoulder at 290 nm with $\varepsilon = 2.1 \times 10^4$ $M^{-1}\cdot cm^{-1}$ due to the oxygen-to-vanadium charge transfer, while that of $\{Et_4N\}_4[HV_{11}O_{29}F_2]$ showed a shoulder at 330 nm with $\varepsilon = 1.1 \times 10^4$ $M^{-1}\cdot cm^{-1}$. Compound $\{Et_4N\}_4[V_7O_{19}F]$ and $\{Et_4N\}_4[HV_{11}O_{29}F_2]$ were orange and red in color and produce respective weak shoulders at 400 nm and 465 nm, respectively (Fig. S6).

Although $\{Et_4N\}_4[V_7O_{19}F]$ and $\{Et_4N\}_4[HV_{11}O_{29}F_2]$ possessed the similar structural components, the electrochemical properties were different from each other (Fig. 5). In the cyclic voltammogram of $\{Et_4N\}_4[V_7O_{19}F]$, an irreversible reductive peak around −1.5 V versus Fc/Fc^+ was recorded and no oxidative peaks appeared in the range. On the other hand, cyclic voltammogram of $\{Et_4N\}_4[HV_{11}O_{29}F_2]$ showed two reductive peaks at −0.71 and –1.5 V versus Fc/Fc^+ and two oxidative peaks at 0.05 and −0.45 V. A reductive peak at −0.71 V and an oxidative peak at −0.45 V were a redox pair. A reductive peak at −1.5 V was irreversible and an oxidative peak at 0.05 was due to the decomposition species by the reduction process (Fig. S7). Considering the structural similarity between $[V_7O_{19}F]^{4-}$ and $[HV_{11}O_{29}F_2]^{4-}$, the redox pair recorded in $[HV_{11}O_{29}F_2]^{4-}$ may be due to redox from the square pyramidal vanadium atoms in the belt layer.

4. Conclusion

Acidification of $[V_4O_{12}]^{4-}$ in the presence of various halide anions revealed that only fluoride anions have the significant effect on the distribution of polyoxovanadate species, giving $[V_7O_{19}F]^{4-}$ and $[HV_{11}O_{29}F_2]^{4-}$ successively. These compounds were characterized by X-ray crystallographic and spectroscopic analyses. The resemblance and difference in the structures and the optical and the electrochemical properties between $[V_7O_{19}F]^{4-}$ and $[HV_{11}O_{29}F_2]^{4-}$ were discussed. The emerging heptavanadate species in an aqueous mixed-solvent-system may help to understand the growth process of metavanadates into decavanadates. A further in vitro and in vivo studies may help to optimize a biological relevant chemistry of vanadium in confined space.

Acknowledgement

This work was supported in part by a Grant-in-Aid for Young Scientists.

Appendix A. Supplementary data

Supplementary data to this article can be found online at (*will be filled in by the editorial staff*). A CIF file of $\{Et_4N\}_4[V_7O_{19}F]$ have been deposited with the number CCDC 1025515. This data can be obtained free of charge from the Cambridge Crystallographic Data Centre via www.ccdc.cam.ac.uk/data_request/cif.

References

[1] D. Rehder, *Bioinorganic Vanadium Chemistry*, John Wiley & Sons, Ltd, 2008, pp. 13-51.

[2] C. C. McLauchlan, D. C. Crans, Dalton Trans. 42 (2013) 11744-11748.

[3] K. Kustin, J. Costa-Pessoa, D. C. Crans (Eds.), Vanadium: The Versatile Metal, ACS Symposium Series, 2007.

[4] M. Aureliano (Ed.), Vanadium Biochemistry, Research Signpost Publs., Kerala, India, 2007.

[5] D. C. Crans, N. E. Levinger, Acc. Chem. Res. 45 (2012) 1637-1645.

[6] M.A. Sedgwick, D.C. Crans, N.E. Levinger, Langmuir 25 (2009) 5496-5503.

[7] N.E. Levinger, L.C. Rubenstrunk, B. Baruah, D.C. Crans, J. Am. Chem. Soc. 133 (2011) 7205-7214.

[8] A. Chatkon, P.B. Chatterjee, M.A. Sedgwick, K.J. Haller, D.C. Crans, Eur. J. Inorg. Chem. 2013 (2013) 1859-1868.

[9] D.C. Crans, B. Baruah, A. Ross, N.E. Levinger, Coord. Chem. Rev. 253 (2009) 2178-2185.

[10] N. Bošnjakovic-Pavlovic, J. Prévost, A. Spasojevic-de Biré, Crystal Growth & Design 11 (2011) 3778-3789.

[11] M. Aureliano, G. Fraqueza, C.A. Ohlin, Dalton Trans. 42 (2013) 11770-11777.

[12] D.C. Crans, K.A. Woll, K. Prusinskas, M.D. Johnson, E. Norkus, Inorg. Chem. 52 (2013) 12262-12275.

[13] M. Aureliano, D.C. Crans, J. Inorg. Biochem. 103 (2009) 536-546.

[14] M. Aureliano, C.A. Ohlin, J. Inorg. Biochem. 137 (2014) 123-130.

[15] N. Steens, A. M. Ramadan, G. Absillis, T. N. Parac-Vogt, Dalton Trans. 39 (2010) 585-592.

[16] L. Pettersson, Coord. Chem. Rev. 237 (2003) 77-87.

[17] I. Andersson, A. Gorzsas, C. Kerezsi, I. Toth, L. Pettersson, Dalton Trans. (2005) 3658-3666.

[18] A. Gorzsas, I. Andersson, L. Pettersson, J. Inorg. Biochem. 103 (2009) 517-526.

[19] K. Okaya, T. Kobayashi, Y. Koyama, Y. Hayashi, K. Isobe, Eur. J. Inorg. Chem. 2009 (2009) 5156-5163.

[20] H. Nakano, T. Ozeki, A. Yagasaki, Acta Cryst. C58 (2002) m464-m465.

[21] *CrystalClear*, version 1.3.5, Rigaku Corporation, Tokyo, Japan.

[22] *CrystalStructure*, version 4.1, Rigaku Corporation, Tokyo, Japan.

[23] Sheldrick, G. M. *Acta Cryst.* A64 (2008) 112-122.

[24] Sheldrick, G. M. *SHELXL2013*. University of Göttingen, Germany, 2013.

[25] Baes, C. F., Jr.; Mesmer, R. E. Hydrolysis of Cations; Wiley & Sons: New York, 1976.

[26] J. Forester, B. Rösner, M. M. Khusniyarov, C. Streb, Chem. Commun. 47 (2011) 3114-3116.

[27] Y. Hayashi, Coord. Chem. Rev. 255 (2011) 2270-2280.

[28] S. Konaka, Y. Ozawa, A. Yagasaki, Inorg. Chem. Commun. 11 (2008) 1267-1269.

[29] K. Kastner, J. T. Margraf, T. Clark, C. Streb, Chem. Eur. J. 20 (2014) 12269-12273.

[30] V. W. Day, W. G. Klemperer, O. M. Yaghi, J. Am. Chem. Soc. 111 (1989) 5959-5961.

[31] N. E. Brese, M. O'Keeffe, Acta Cryst. B47 (1991) 192-197.

[32] I. Omri, M. Graia, T. Mhiri, J. Clust. Sci. (2014) in press. DOI: 10.1007/s10876-014-0768-3

[33] A. Müller, J. Meyer, H. Bögge, A. Stammler, A. Botar, Chem. Eur. J. 4 (1998), 1388-1397.

[34] C. Ninclaus, D. Riou, G. Férey, Chem. Commun. (1997) 851-852.

[35] M. I. Khan, Q. Chen, F. Höpe, S. Parkin, C. J. O'Connor, J. Zubieta, Inorg. Chem. 32 (1993) 2323-2937.

[36] J. Spandl, I. Brüdgam, Hans Hartl, Zeit. Anorg. Allgem. Chem. 629 (2003) 539-544.

[37] D. Riu, F. Taulelle, G. Férey, Inorg.Chem. 35 (1996) 6392-6395.

[38] A. Müller, R. Rohlfing, E. Krickemeyer, H. Bögge, Angew. Chem. Int. Ed. 32 (1993) 909-912.

[39] C.-D. Zhang, S.-X. Liu, B. Gao, C.-Y. Sun, L.-H. Xie, M. Yu, J. Peng, Polyhedron 26 (2007) 1514-1522.

[40] E. E. Hamilton, P. E. Fanwick, J. J. Wilker, J. Am. Chem. Soc. 124 (2002) 78-82.

[41] V. W. Day, W. G. Klemperer, O. M. Yaghi, J. Am. Chem. Soc. 111 (1989) 4518-4519.

[42] Q. Wu, X. Hao, X. Feng, Y. Wang, Y. Li, E. Wang, X. Zhu, X. Pan, Inorg. Chem. Commun. 22 (2012) 137-140.

[43] Y.-P. Xie, T. C. W. Mak, Chem. Commun. 48 (2012) 1123-1125.

[44] Y. Hayashi, N. Miyakoshi, T. Shinguchi, A. Uehara, Chem. Lett. (2001) 170-171.

[45] S. Inami, M. Nishio, Y. Hayashi, K. Isobe, H. Kameda, T. Shimoda, Eur. J. Inorg. Chem. (2009) 5253-5258.

[46] M. Nishio, S. Inami, Y. Hayashi, Eur. J. Inorg. Chem. (2013) 1876-1881.

[47] M. Nishio, S. Inami, M. Katayama, K. Ozutsumi, Y. Hayashi, Inorg. Chem. 51 (2012) 754-793.

[48] Y.-F. Qi, C.-P. Lv, Y.-G. Li, E.-B. Wang, J. Li, X.-L. Song, Inorg. Chem. Commun. 13 (2010) 384-387.

[49] H. Reuter, M. Izaaryene, Inorg. Chim. Acta 363 (2010) 4277-4281.

[50] A. Seliverstov, J. Forster, M. Heiland, J. Unfriend, C. Streb. Chem. Commun. 50 (2014) 7840-7843.

[51] J. M. Cameron, G. N. Newton, C. Busche, D.-L. Long, H. Oshio, L. Cronin, Chem. Commun. 49 (2013) 3395-3397.

[52] T. Kobayashi, S. Kuwajima, T. Kurata, Y. Hayashi, Inorg. Chim. Acta 420 (2014) 69-74.

[53] H. T. Evans, Jr. Inorg. Chem. 5 (1966) 967-977.

[54] V. W. Day, W. G. Klemperer, D. J. Maltbie, J. Am. Chem. Soc. 109 (1987) 2991-3002.

[55] K. Katner, B. Puscher, C. Streb, Chem. Commun. 49 (2013) 140-142.

Table 1

Selected average bond lengths (Å) for $[V_7O_{19}F]^{4-}$, $[V_7O_{18}F(CH_2)_3CCH_2OH]^{4-}$ [33], and $[HV_{11}O_{29}F_2]^{4-}$ [19].

	$[V_7O_{19}F]^{4-}$	$[V_7O_{18}F(CH_2)_3CCH_2OH]^{4-}$	$[HV_{11}O_{29}F_2]^{4-}$
V=O	1.62	1.62	1.60
V_{bottom}−μ-O(−V_{bottom})	1.83	2.03	1.83
V_{bottom}−μ-O(−V_{middle})	1.97	1.98	1.99
V_{middle}−μ-O(−V_{bottom})	1.72	1.71	1.83
V_{middle}−μ-O(−$V_{bottom'}$)			2.00
V_{middle}−μ-O(−V_{top})	1.84	1.83	
V_{top}−μ-O	1.76	1.75	
$V_{bottom}\cdots F$	2.31	2.21	2.21
$V_{middle}\cdots F$	2.76	2.94	3.06
$V_{middle}\cdots F'$			3.26
$V_{top}\cdots F$	2.97	3.24	
$V_{bottom}\cdots V_{bottom}$	3.15	3.33	3.09
$V_{bottom}\cdots V_{middle}$	3.78	3.31	3.49
$V_{middle}\cdots V_{middle'}$			3.10
$V_{middle}\cdots V_{middle}$	4.54	4.66	4.92
$V_{middle}\cdots V_{middle'}$			2.88
$V_{middle}\cdots V_{top}$	3.35	3.38	

Figure legends

Fig. 1. ^{51}V NMR spectra in a mixed solvent of CD_3CN and D_2O (3:1, v/v) after the addition of (a) 0, (b) 0.57, (c) 1.1, and (d) 1.7 equivalents of TsOH with respect to $\{Et_4N\}_4[V_4O_{12}]$. Signals around −585 and −596 ppm were due to $[V_4O_{12}]^{4-}$ and $[V_5O_{15}]^{5-}$, respectively. Signals at −423, −500, and −519 ppm were due to a decavanadate. Signals at −601 and −608 ppm were probably due to $[V_{12}O_{32}(CH_3CN)]^{4-}$.

Fig. 2. ^{51}V NMR spectra in the presence of 0.8 equivalents of $\{n\text{-}Bu_4N\}F$ in a mixed solvent of CD_3CN and D_2O (3:1, v/v) after the addition of (a) 0, (b) 0.57, (c) 1.1, (d) 1.7, (e) 2.3, (f) 2.8, and (g) 3.4 equivalents, of TsOH with respect to $\{Et_4N\}_4[V_4O_{12}]$. Signals around −585 and −596 ppm were due to $[V_4O_{12}]^{4-}$ and $[V_5O_{15}]^{5-}$, respectively. Signals at −460, −547, and −611 ppm were due to $\{Et_4N\}_4[V_7O_{19}F]$. Signals at −471, −474, −492, −505, −530, and −540 ppm were due to $\{Et_4N\}_4[HV_{11}O_{29}F_2]$.

Fig. 3. ORTEP representation of (a) top view and (b) side view of $[V_7O_{19}F]^{4-}$ (50% probability displacement ellipsoids).

Fig. 4. Ball and stick representations of (a) $[V_7O_{19}F]^{4-}$ and (b) $[HV_{11}O_{29}F_2]^{4-}$. The colored parts $[V_6O_{15}F]^-$ in $[V_7O_{19}F]^{4-}$ and $[HV_{11}O_{29}F_2]^{4-}$ resemble each other. Each sphere represents oxygen (red and dark gray spheres), vanadium (orange and light gray spheres), fluorine (green and the largest gray spheres) and hydrogen atoms (the smallest gray sphere).

Fig. 5. (A) ^{51}V NMR and (B) ^{19}F NMR spectra of (a) $\{Et_4N\}_4[V_7O_{19}F]^{4-}$ and (b) $\{Et_4N\}_4[HV_{11}O_{29}F_2]$ in a mixed solvent of propylene carbonate and dichloromethane-d_2 (1:1, v/v).

Fig. 6. Cyclic voltammograms of (a) $\{Et_4N\}_4[V_7O_{19}F]$ and (b) $\{Et_4N\}_4[HV_{11}O_{29}F_2]$ in a mixed solvent of propylene carbonate and dichloromethane (1:1, v/v). Scan rate was 100 mV/sec. The supporting electrolyte was $\{n\text{-}Bu_4N\}BF_4$. Reduction peaks **I** and **III** were irreversible. Peaks **II** and **II'** were redox pair. The asterisk indicates the peak due to the decomposition species by the reduction process

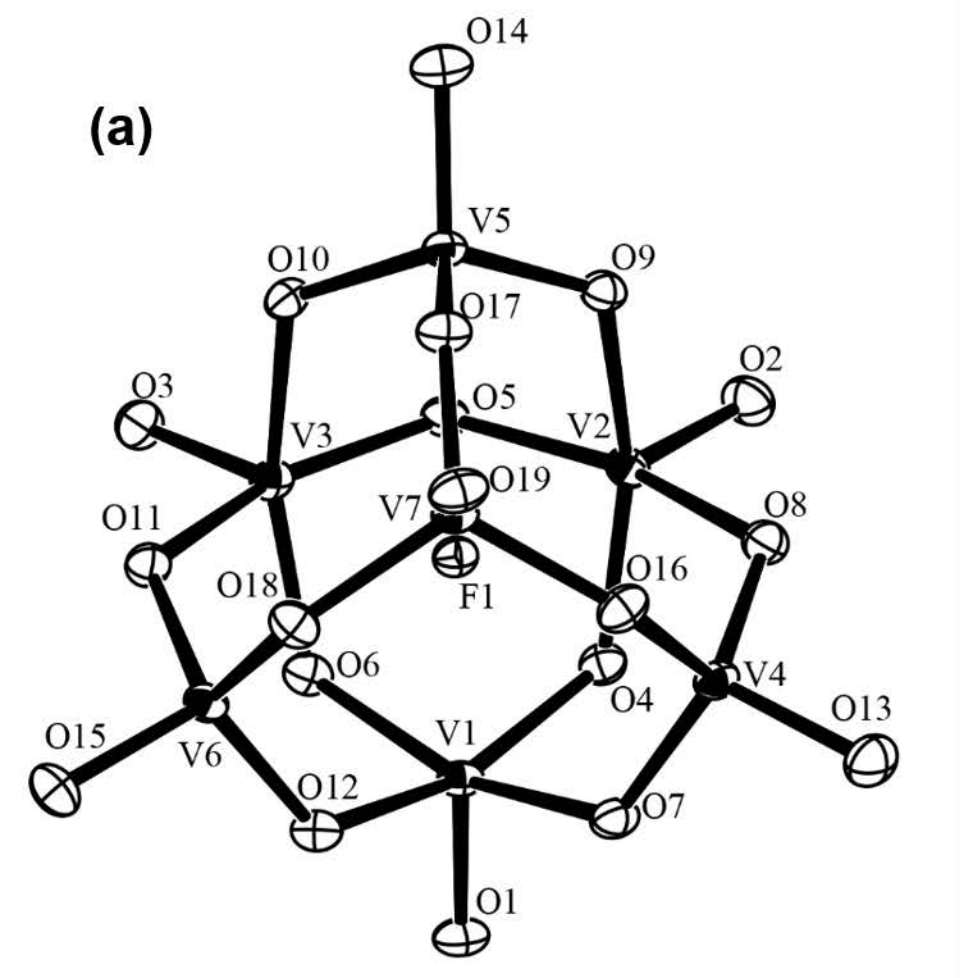
(a)
O14
V5
O10
O9
O17
O2
O3
O5
V3
V2
O19
V7
O11
O8
O18
F1
O16
O6
V4
O4
O13
O15
V6
V1
O12
O7
O1

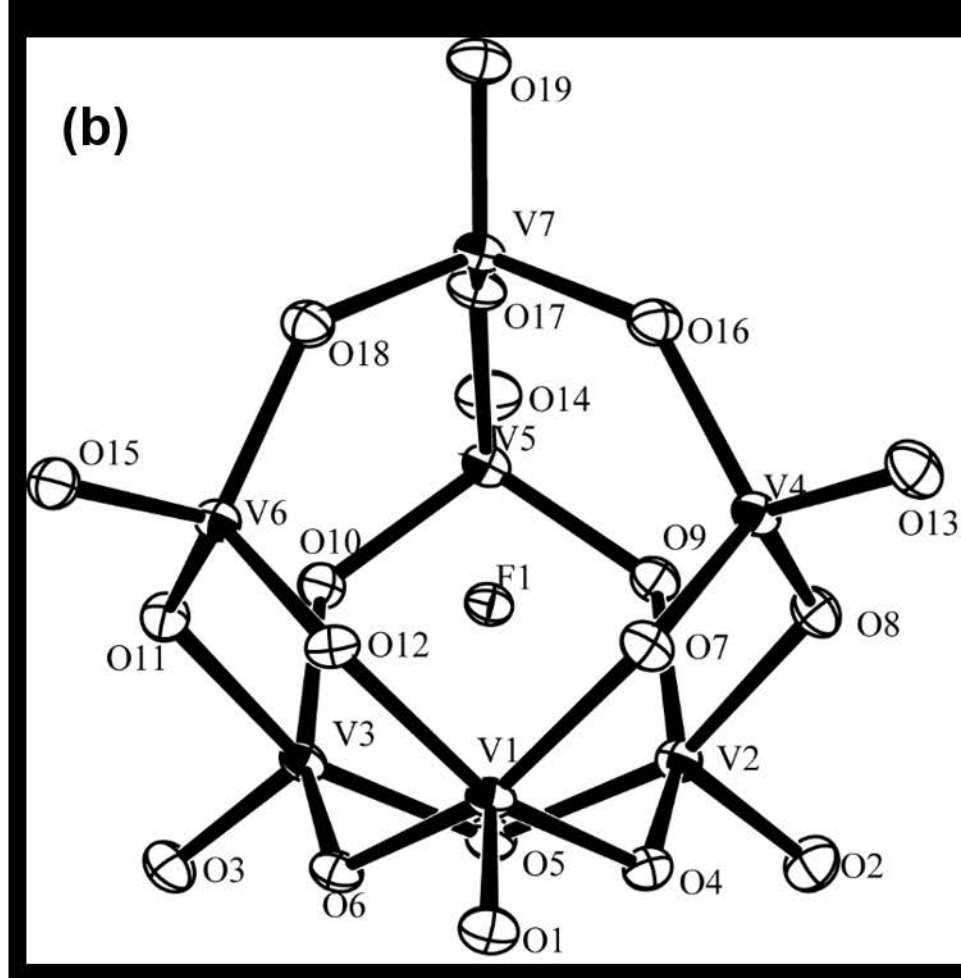
(b)
O19
V7
O17
O16
O18
O14
O15
V5
V4
O13
V6
O10
O9
F1
O8
O11
O12
O7
V3
V1
V2
O3
O5
O4
O2
O6
O1

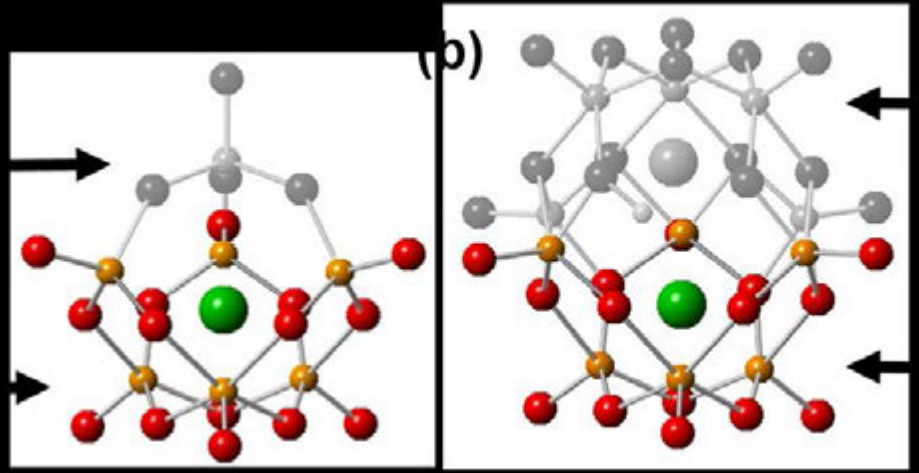
(b)

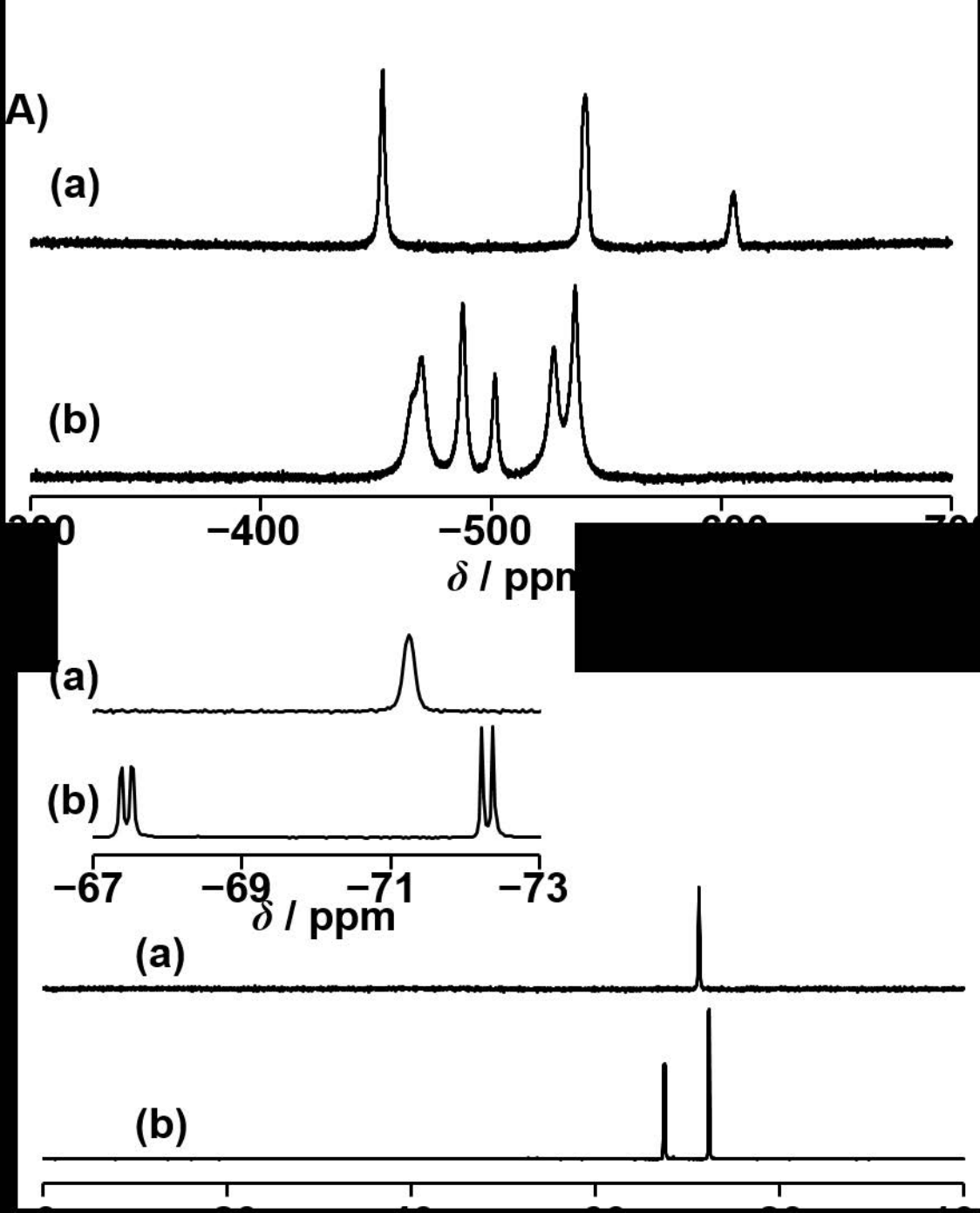
A)
(a)
(b)
−400
−500
δ / ppm
(a)
(b)
−67
−69
−71
−73
δ / ppm
(a)
(b)

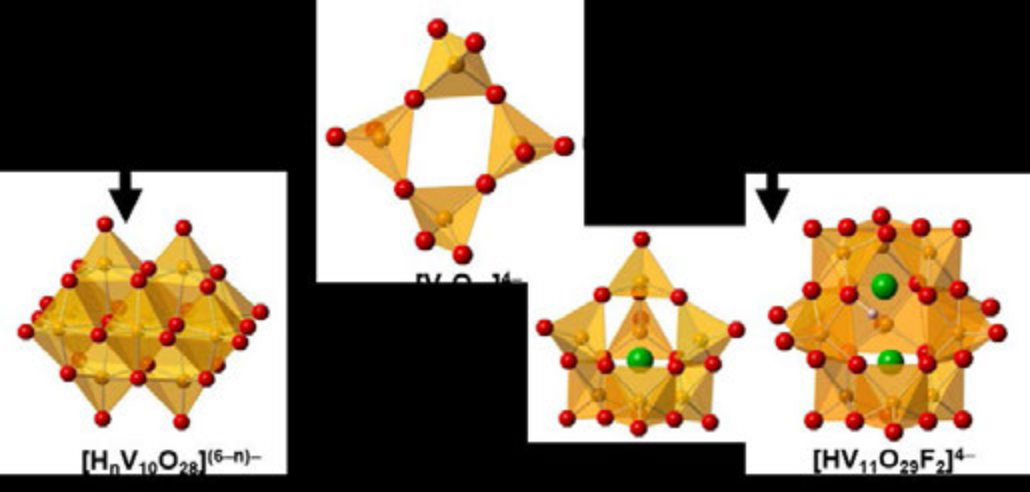
$[H_nV_{10}O_{28}]^{(6-n)-}$
$[HV_{11}O_{29}F_2]^{4-}$